frontiers | Frontiers in Energy Research

ORIGINAL RESEARCH
published: 23 August 2022
doi: 10.3389/fenrg.2022.919878

The Effect of Trace Ions on the Performance of Reverse Electrodialysis Using Brine/Seawater as Working Pairs

Zhihao Wang, Jianbo Li, Hao Wang, Mengqi Li, Lingjie Wang and Xiangqiang Kong*

Department of Thermal Engineering, School of Mechanical and Electronic Engineering, Shandong University of Science and Technology, Qingdao, China

Harvesting the salinity gradient power (SGP) between concentrated brine discharged from seawater desalination installations and seawater and converting into electric energy by reverse electrodialysis (RED) is a promising technique. However, trace ions in brine and seawater may affect the performance of the RED stack, and little attention has been focused on this issue. Therefore, the influences of trace ions in seawater and concentrated brine are analyzed in this work. The effects of these ions on power density, open-circuit voltage, and internal resistance of the RED stack are analyzed by configuring manual seawater and concentrated brine including K^{1+}, Mg^{2+}, SO_4^{2-}, and Ca^{2+}. Experimental results show that divalent ions (Mg^{2+}, SO_4^{2-}, and Ca^{2+}) can significantly increase the internal resistance of the RED stack and reduce power density. Mg^{2+} especially has the largest reduction in the output power of the stack. Oppositely, potassium ions (K^{1+}) in feed solutions will reduce the internal resistance and improve power output. In addition, increasing the salinity gradient of feed solutions, temperature, and flow rate can increase open-circuit voltage and power density, and reduce inner power consumption of the RED stack. This study can provide references for the recovery of SGP in seawater desalination plants.

Keywords: reverse electrodialysis, salinity gradient power, power production, trace ions, desalination

OPEN ACCESS

Edited by:
Yun-Xiao Wang,
University of Wollongong, Australia

Reviewed by:
Xi Wu,
Dalian University of Technology, China
Bing Zhang,
Shenyang University of Technology, China
Xia Sun,
Jiangsu Ocean Universiity, China

****Correspondence:***
Jianbo Li
ljb_198504@163.com

Specialty section:
This article was submitted to Electrochemical Energy Conversion and Storage, a section of the journal Frontiers in Energy Research

Received: *14 April 2022*
Accepted: *09 June 2022*
Published: *23 August 2022*

Citation:
Wang Z, Li J, Wang H, Li M, Wang L and Kong X (2022) The Effect of Trace Ions on the Performance of Reverse Electrodialysis Using Brine/Seawater as Working Pairs. Front. Energy Res. 10:919878. doi: 10.3389/fenrg.2022.919878

1 INTRODUCTION

Salinity gradient power (SGP) is a chemical store of energy formed from the potential difference existing in the confluence of rivers and seas (Roldan-Carvajal et al., 2021); approximately 30 TWh of SGP can be harvested from the principal rivers of the world (Jang et al., 2020). However, large-scale utilization of this energy is still limited due to the poor net power density of natural water bodies (Tufa et al., 2018). The method of converting the energy to electric energy mainly includes pressure-retarded osmosis (PRO) (Achilli and Desalination, 2010; Ngai and Menachem et al., 2012; Helfer et al., 2014) and reverse electrodialysis (RED) (Simões et al., 2020; Kim et al., 2021). Of these methods, RED is a relatively feasible and potential conversion technology owing to its simple and compact assembling (Tedesco et al., 2017), and has drawn some attention from researchers.

Most research is focused on NaCl solution based on the RED model and experiment due to the complexity and heterogeneity of natural water components (Ortiz-Imedio et al., 2019; Jin et al., 2021). When NaCl solution is used as a working fluid, the internal resistance of the RED stack is very low (Moreno et al., 2018), and the maximum energy conversion efficiency of the stack can reach 83%

(Post et al., 2008; Hu et al., 2020). Moreover, concentrations, temperatures, and flow velocity of feed solutions strongly affect the power density (Mei and Tang, 2017; Hu et al., 2019). In a single RED stack, a high-power density of 3.0 W/m^2 can be achieved under the conditions of high concentration gradients and elevated temperatures (Zhu et al., 2015; Hulme et al., 2020). However, when natural seawater is used, the performance of the stack is not ideal (Chon et al., 2020). Differently from pure NaCl solution, natural seawater contains multiple ions, which affect the performance of RED stack (Vermaas et al., 2013; Choi et al., 2022). It is found that multiple ions are the principal reason for the low performance of the stack (Avci et al., 2018). Many scholars attempted to study the effect of different ions in seawater on the performance of RED stack.

Tedesco et al. (Merino-Garcia and Velizarov, 2021) found maximum power density of the RED stack only reached 1.6 W/m^2 when nature river water and seawater were used as feed solutions, which was far lower than the 2.7 W/m^2 of NaCl solutions with the same concentration. The reason for the power reduction is caused by multiple ions in the natural feed solutions (Pintossi et al., 2021). The inner resistance of $MgCl_2$ solution with the same molar concentration of NaCl solution increased three times (Avci et al., 2016). Vermaas et al. (2014) concluded that the membrane penetration was more obvious in the presence of Mg^{2+} by analyzing the stack performance of NaCl solution and $MgSO_4$ solution. They found that multivalent ions could reduce the electromotive force and increase the internal resistance of the stack. Jan et al. (Post et al., 2009) conducted an experiment by using standard grade ion exchange membrane and monovalent selective membrane, and investigated whether SO_4^{2-} or Mg^{2+} could increase the resistance of the stack and reduce the electromotive force of the stack. The reason for this phenomenon is the upward transportation of the multivalent ions (Moya, 2017; Pintossi et al., 2020). Rijnaarts et al. (2017) found that divalent cations could increase the non-ohmic resistance and reduce the open circuit voltage of the stack by adding Mg^{2+} and Ca^{2+} into NaCl solution.

The above studies are based on a combination of seawater and river water (Hong et al., 2014; Avci et al., 2018), and the combination of concentrated seawater and seawater are not involved. There are only a few studies on the influence of multiple ions on the stack when concentrated seawater and seawater are used as feed solutions. Guo et al. (2018) found the influence order of ions coexisting with NaCl is Ca^{2+} > Mg^{2+} (>SO_4^{2-}) > K^+ in a concentrated seawater and seawater combination. In their study, the concentration of NaCl is set to 66 g/L. However, a wider salinity range needs to be studied if the RED stack is used to capture the SGP between seawater and concentrated brine discharged from seawater desalination installation.

In our previous study, the SGP capture between concentrated brines from desalination and seawater for power production was proposed within a wide salinity range (Jianbo et al., 2021). The influences of insoluble substances in natural seawater are also investigated (Kang et al., 2022). However, the influence of various ions in natural seawater needs to be investigated in a wide concentration range. Therefore, this work aimed to study the contribution of various ions (K^+, Mg^{2+}, SO_4^{2-}, and Ca^{2+}) in concentrated brine and seawater to the performance of RED stack by adding one or various ions to feed solutions. A performance evaluation index including power density, open-circuit voltage, internal resistance, and other parameters of the RED stack are compared under different ion combinations. This work can provide some guidance for the utilization of SGE.

2 EXPERIMENT

Figure 1A illustrates the RED experimental test diagram based on different concentrations of brine, and **Figure 1B** shows the actual setup. As shown, the experimental system is mainly composed of a RED stack, feed pumps, and testing instruments. The principal test instruments are listed in **Table 1**. The principal structural parameters of the stack are given in **Table 2**. **Table 3** shows the properties of ion exchange membranes produced by the Fujifilm company. The solvent used is of analytical grade (Sinopharm Chemical ReagentCo., Ltd.), with a content greater than 99.5%.

A magnetic heater and a constant temperature water bath are used to heat the feed solution and maintain it at the desired temperature, respectively. The temperature difference of the solution after passing through the stack is less than 1°C. Two peristaltic pumps with metering functions are used to draw feed solutions to the RED stack and record their flow rate. A peristaltic pump is used to circulate the electrode rinse solution in the cathode, anode chamber, and the reservoir. Two differential pressure sensors are used to test the flow resistances of feed solutions. A conductivity meter is used to test the conductivity of feed solutions and discharge solutions. A data acquisition unit is used to receive the temperature signal, flow signal, and pressure signal. An electrochemical station coupling with a current amplifier is used to test the voltage and current of the RED stack.

Experimental procedures are described as follows. Sodium chloride solution with the concentration of 0.5 and 2.5 mol/L were prepared as the basic solution, in which 0.5 mol/L was used to simulate the salinity of seawater and 2.5 mol/L was the maximum salinity of brine discharged from desalination unit. To study the influence of trace ions in seawater on the stack, different kinds of ions (K^+, Mg^{2+}, SO_4^{2-}, and Ca^{2+}) were added to the basic solution. In the experiment, $K_3Fe(CN)_6$ solution of 0.3 mol/L and $K_4Fe(CN)_6$ solution of 0.26 mol/L were used as electrode leaching solution, and 1.5 mol/L sodium chloride was used as supporting electrolyte. Ions in the experiment are listed in **Table 4**.

On the basis of the above experimental data, the performances of a RED stack can be expressed as follows.

2.1 Output Voltage

$$U = OCV - IR_i \tag{1}$$

where, U is output voltage of the RED stack, V. I is the closed-circuit current, A.

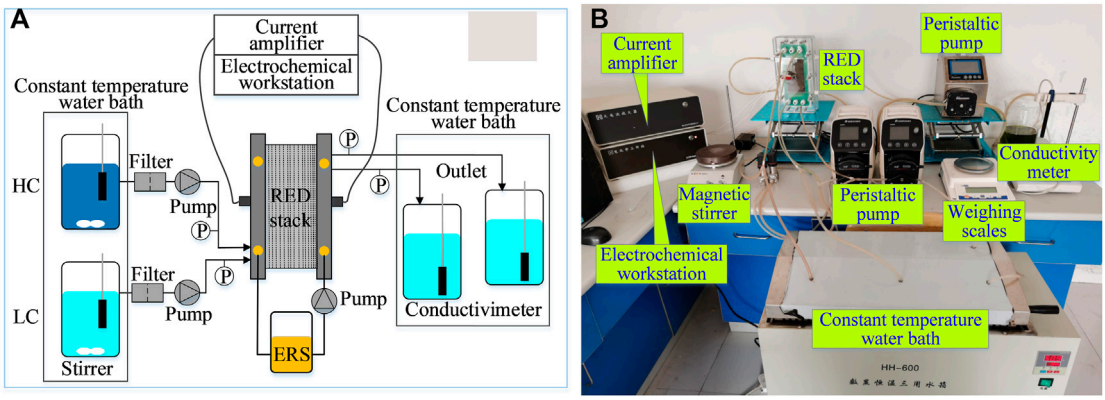

FIGURE 1 | Test system of the RED stack experiment.

TABLE 1 | Main instruments.

Numbers	Instruments	Specifications
1	Magnetic stirrer	JB-2A
2	Electronic balance	LabN6
3	Ultrapure water filter	UPT-I-10T
4	Conductivity meter	FE38-Standard
5	Electrochemical workstation	CHI-660E
6	Constant temperature water bath	HH-600
7	Electronic balance	XY-1000-2C

TABLE 2 | Principal structure of the RED stack.

Components	Descriptions	Value	Unit
RED stack	Cell unit	10	—
	Width	300	mm
	Length	200	mm
Electrode plate	Width	118	mm
	Length	65	mm
Spacer	Number	22	—
	Thickness	0.3	mm

TABLE 3 | Properties of ion exchange membranes.

Properties	AEM/CEM-type II	Units
Membrane type	Homogeneous	—
Thickness	160	μm
Permselectivity (NaCl)	95–96	%
Permselectivity (KCl)	95–96	%
Electrical resistance (NaCl)	3.5	Ω·cm^2
Electrical resistance (KCl)	6.1	Ω·cm^2
Water permeation	3/3.5	ml/bar·m^2·hr

The internal resistance of the stack includes ohmic resistance and non-ohmic resistance. Non-ohmic resistance includes surface resistance caused by a concentration change in body fluid (Vermaas et al., 2011a; Vermaas et al., 2011b). Inner resistance of the RED stack can be expressed as

TABLE 4 | Ion concentration in feed solution.

Ion type (solvent)	Dilute brine (mol/L)	C_H = 1 (mol/L)	C_H = 2 (mol/L)	C_H = 3 (mol/L)	C_H = 4 (mol/L)
Na^+ (NaCl)	0.500	1.000	1.500	2.000	2.500
Mg^{2+} ($MgCl_26H_2O$)	0.054	0.108	0.162	0.216	0.270
Ca^{2+} ($CaCl_2$)	0.011	0.022	0.033	0.044	0.055
K+ (KCl)	0.010	0.020	0.030	0.040	0.050
SO_4^{2-} (Na_2SO_4)	0.028	0.056	0.084	0.112	0.14

$$R_i = \frac{(OCV - U)}{I} \tag{2}$$

2.2 Power of a Reverse Electrodialysis Stack

$$P = UI \tag{3}$$

Power density of a RED stack is defined as

$$P_d = \frac{P}{A_{RED}} \tag{4}$$

A_{RED} is the effective area of all battery cells in stack, m^2.

The electromotive force generated at position x in the stack is equal to the sum of the electromotive forces of anion and cation exchange membranes. It can be expressed as

$$E_{cell}(x) = E_{AEM}(x) + E_{CEM}(x) \tag{5}$$

Nernst potential predicts the electromotive at x position on both sides of the ion exchange membrane

$$E_{AEM}(x) = \alpha_{AEM}\frac{RT}{zF}\ln\left(\frac{\gamma_{HC} - C_{HC} -}{\gamma_{LC} - C_{LC}-}\right) \tag{6}$$

$$E_{CEM}(x) = \alpha_{CEM}\frac{RT}{zF}\ln\left(\frac{\gamma_{HC} + C_{HC} +}{\gamma_{LC} + C_{LC}+}\right) \tag{7}$$

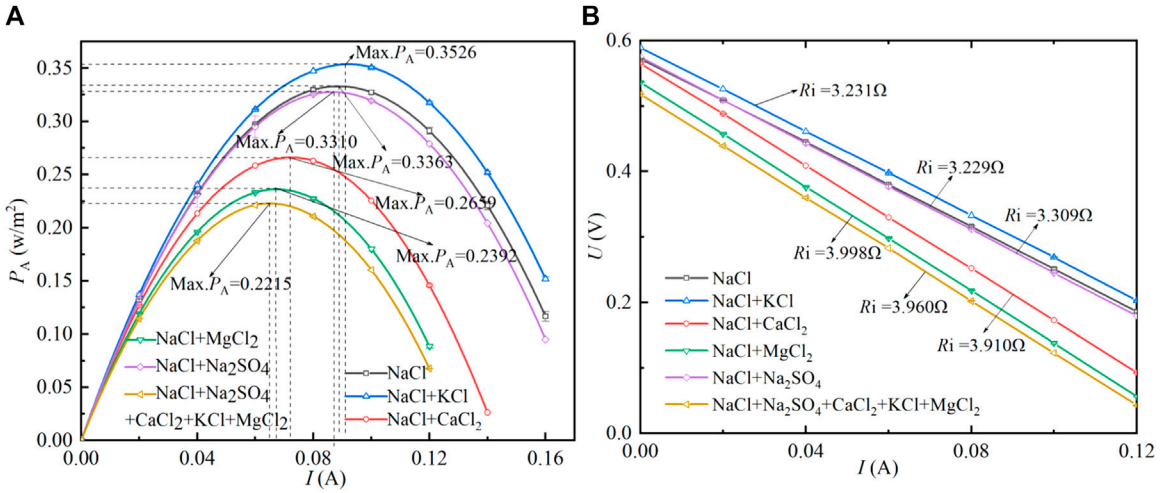

FIGURE 2 | Performance variation of the RED stack with the current. Feed temperature is set as 19°C, flow rate is 50 ml/min. 0.270 mol/L $MgCl_2$, 0.055 mol/L $CaCl_2$, 0.050 mol/L KCl, and 0.140 mol/L Na_2SO_4 were added to 2.5 mol/L NaCl solution. 0.054 mol/L $MgCl_2$, 0.011 mol/L $CaCl_2$, 0.010 mol/L KCl, and 0.025 mol/L Na_2SO_4 were added to 0.5 mol/L NaCl solution.

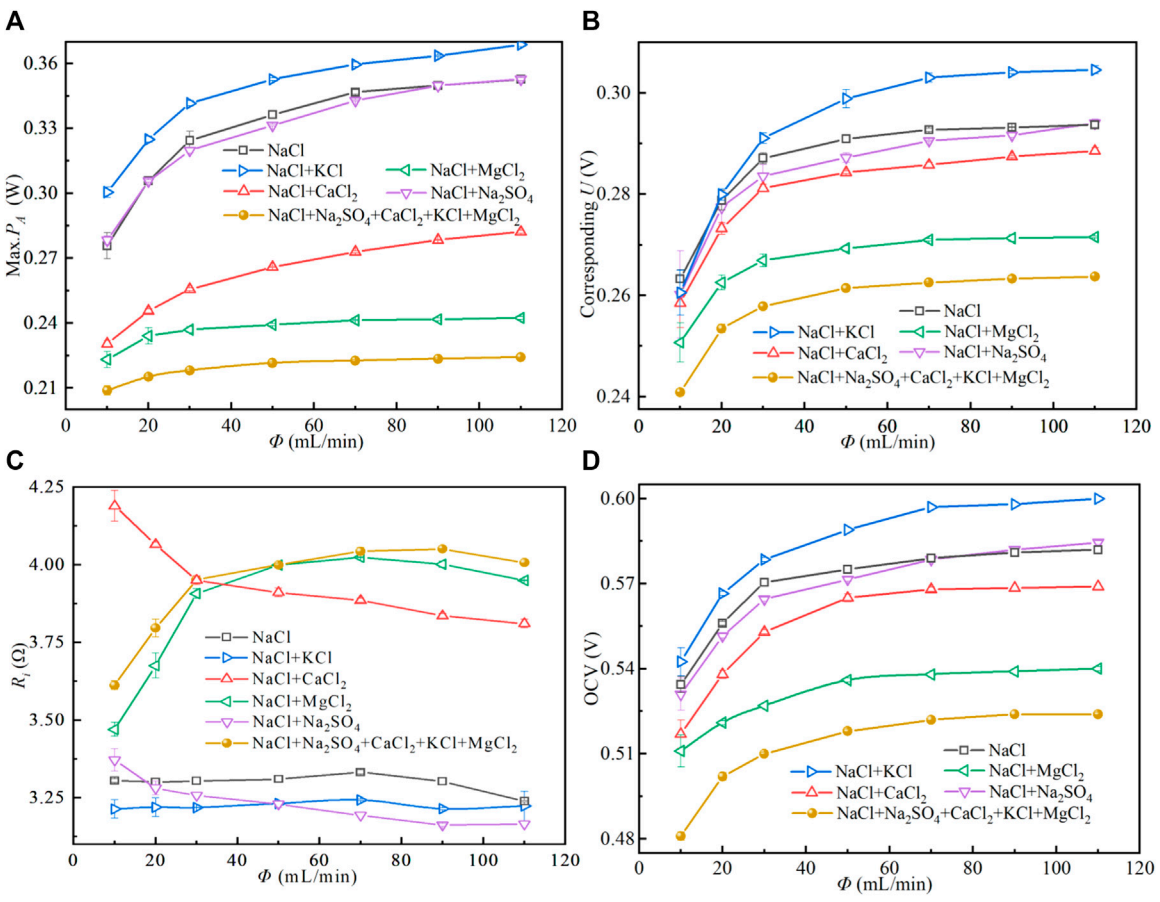

FIGURE 3 | Performance variation of the RED stack with the flow rate (Φ). Feed temperature is set as 19°C and concentrations of trace ions are as same as that in **Figure 2**.

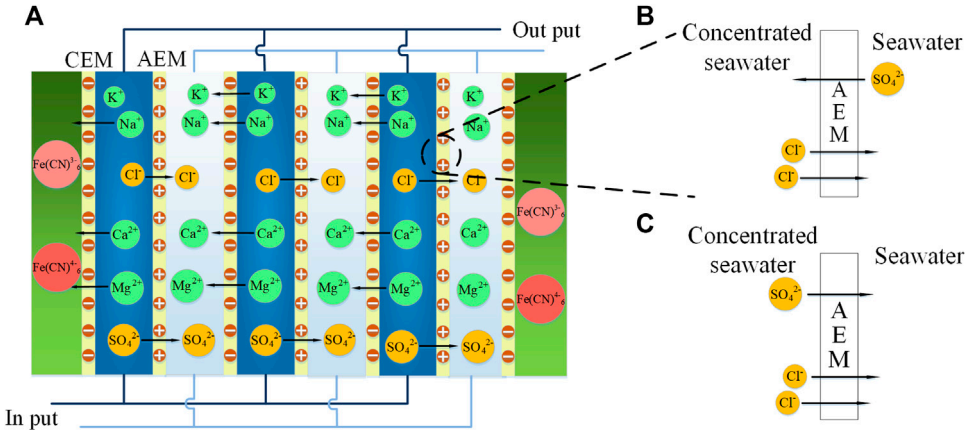

FIGURE 4 | Schematic diagram of ion influence mechanism.

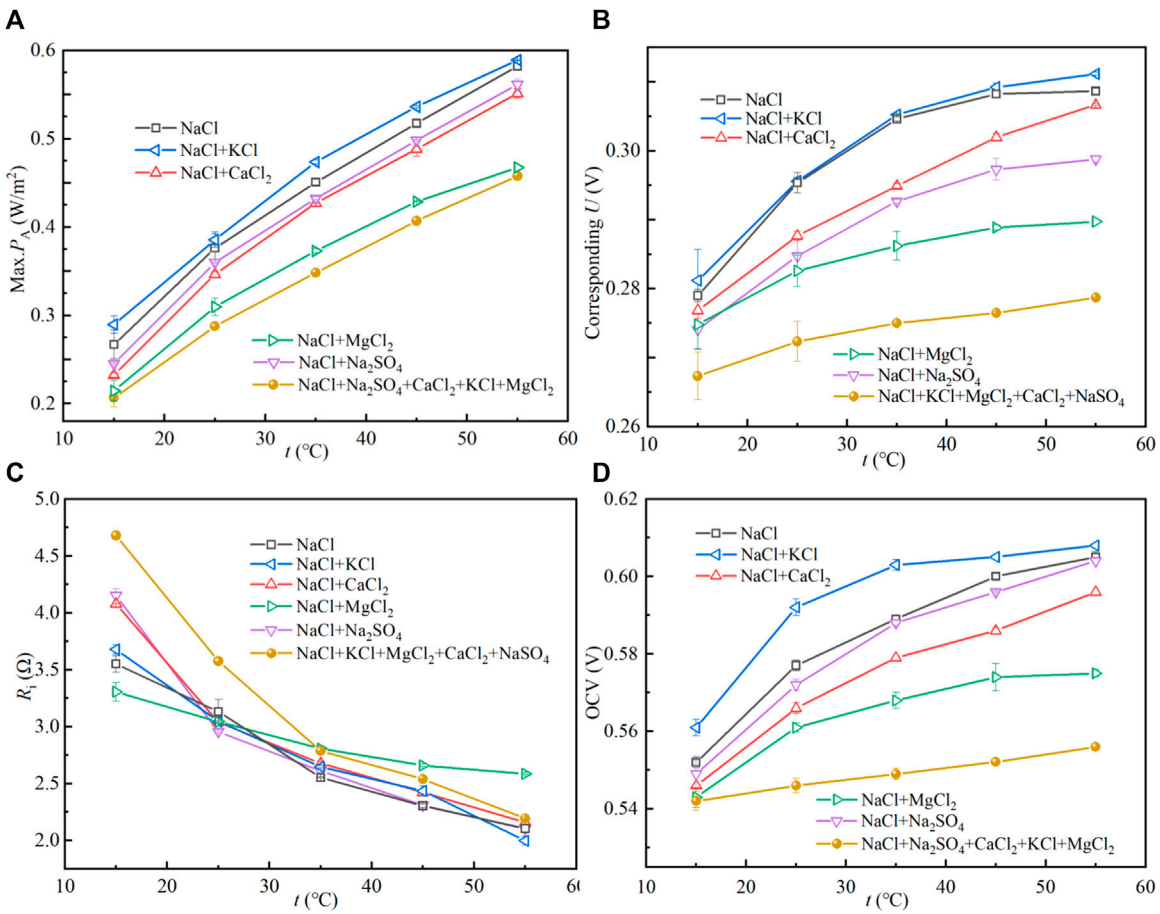

FIGURE 5 | Performance variation of the RED stack with the feed temperature. Flow rate is 50 ml/min, and concentrations of trace ions are the same as that in **Figure 2**.

α_{AEM} and α_{CEM} represent the selective permeability coefficients of anion and cation exchange membrane, respectively. R is the gas constant. T is Kelvin temperature. Z is the ionic valence state. F is the Faraday constant. Γ is the average ionic activity coefficient of the solution. In practice, the selective permeability coefficient of ion exchange

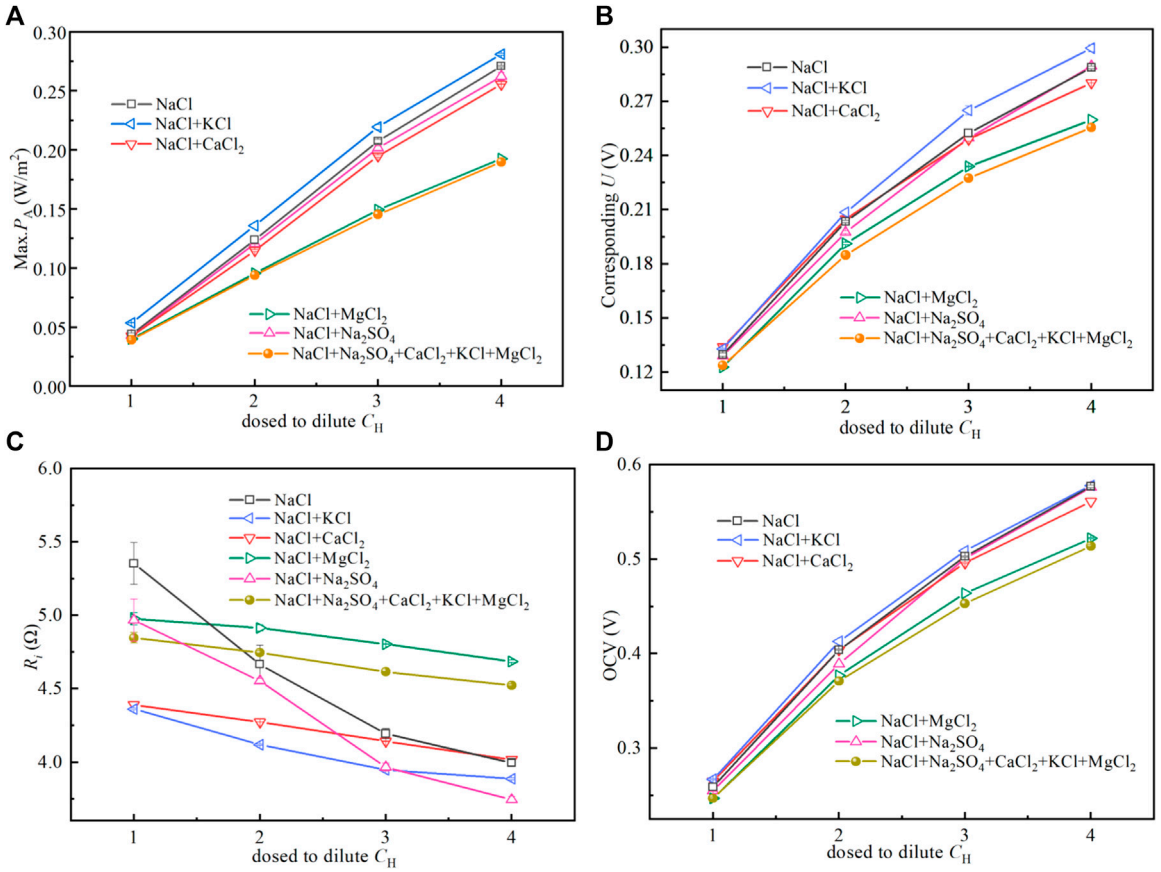

FIGURE 6 | Performance variation of the RED stack with the concentration of the brine (CH). The experiment was carried out at t = 14°C, Φ = 50 ml/min. In the experiment, one or all of 0.270 mol/L $MgCl_2$, 0.055 mol/L $CaCl_2$, 0.050 mol/L KCl, and 0.140 mol/L Na_2SO_4 were added to 2.5 mol/L sodium chloride solution, one or all of 0.054 mol/L $MgCl_2$, 0.011 mol/L $CaCl_2$, 0.010 mol/L KCl and 0.025 mol/L Na_2SO_4 were added to 0.5 mol/L sodium chloride solution. They are used as feed solutions.

membrane may change due to the influence of temperature and humidity.

3 RESULTS AND ANALYSIS

3.1 The Influence of Adding Trace Ions on the Performance of the Reverse Electrodialysis stack

Figures 2A,B shows the variation law of the power density (P_A) and voltage of the RED stack (corresponding U) with the current (I) after adding different trace ions. The slope of the curve in **Figure 2B** represents the internal resistance (R_i) of the stack, and the open circuit voltage (OCV) is the voltage when the current is zero. It can be found that the addition of KCl can improve the output performance of the stack. Compared with pure NaCl solution, the maximum P_A and OCV are increased by 4.8% and 0.014 V, respectively, while R_i changes little. This is related to the ionic group of Fujifilm type II, which is designed for the exchange of monovalent ions. Therefore, adding KCl to the basic solution can improve the performance of the stack. Different from the addition of KCl, the maximum P_A in **Figure 2A** is decreased by 1.5%, 20.9%, 28.9%, and 34.1% respectively after adding Na_2SO_4, $CaCl_2$, $MgCl_2$, and all ions to the basic solution. This effect is the same as the research of Hong, who used seawater and river water as feed solution (Hong et al., 2014). In addition, R_i changes little (increased by 0.08 Ω) when Na_2SO_4 is added to the basic solution. The explanation for this phenomenon is that the addition of SO_4^{2-} only affects the membrane potential, and the uphill transport of magnesium ions will be offset by the added Na^+. It can also be found in **Figure 2B** that the addition of Mg^{2+} and Ca^{2+} are the principal reasons for the increase of R_i, which is increased by 0.781 and 0.769 Ω respectively compared with pure NaCl solution. This is due to the low diffusion coefficient or the shielding effect of Mg^{2+} and Ca^{2+} on the ionic groups on the cation exchange membrane (Vermaas et al., 2014). This also proves that the membrane resistance of CEM is more sensitive to multivalent ions. Therefore, the divalent cations in the feed solution should be eliminated or the structure of CEM changed by adding some groups that hinder the passage of multivalent ions to the CEM. R_i is increased by 0.731 Ω when

all ions are in the basic solution, which is lower than adding Mg^{2+} or Ca^{2+} alone. This is due to the rise of conductivity of feed solutions when all ions are added (Post et al., 2009).

3.2 Influencing Factors Analysis

3.2.1 Influence of Flow Rate

As shown in **Figure 3A**, the max. P_A has a large increment of 17.7% with flow rate (Φ) increasing from 10 to 30 ml/min when the feed solution is the base solution, while it increases 9.0% with Φ increasing from 30 to 110 ml/min. As shown in **Figure 3D**, OCV also increases with the increase of Φ. The principal reason is that the concentration polarization is weakened and the salinity difference on both sides of the exchange membrane is more stable, so as to increase the P_A when Φ is high [39]. However, excessive Φ will cause the loss of pump power. Therefore, selecting the appropriate solution flow rate is conducive to improving the net power density of the stack. As shown in **Figure 3C**, R_i changes very little when Φ varies. In addition, the phenomenon of high R_i and low P_A are also found in **Figures 3A,C**, which is in line with the influence law of divalent ions on the stack. Inside, the Max. P_A is reduced by 50% after adding $MgCl_2$ to the basic solution, which is consistent with the prediction of Diego (Pintossi et al., 2021).

As shown in **Figure 3A**, increasing the Φ can increase the Max. P_A of the stack. As shown in **Figure 3C**, the feed solution containing Ca^{2+} and Mg^{2+} shows high R_i, resulting in a lower Max. P_A is caused by the uphill transportation of multivalent ions (Moreno et al., 2018). Uphill transportation will lead to the exchange of some multivalent ions and monovalent ions. For example, in the mixed solution of NaCl and Na_2SO_4, one SO_4^{2+} and two Cl^- exchange due to the electrochemical potential difference (Vermaas et al., 2014). This part of ion exchange will not generate Max. P_A in an external circuit is shown in **Figures 4A,B**. After the uphill transportation is balanced, the electromotance is generated by the forward transportation, as shown in **Figures 4A,C**. As shown in **Figure 3B**, the increase of Φ leads to a higher Max. P_A, and the corresponding U at the Max. P_A also increases. As shown in **Figure 3C**, the R_i increases with the increase of Φ in the presence of Mg^{2+}. This phenomenon may be caused by the shielding effect of Mg^{2+} on the ion groups on the ion exchange membrane. The greater the Φ, the more obvious the shielding effect. The addition of Ca^{2+} to NaCl solution resulted in high R_i, but the R_i decreased with the increase of Φ. As shown in **Figure 3D**, with the increase of Φ, the concentration polarization in the stack is reduced, which causes the OCV to increase.

3.2.2 Influence of Feed Temperature

Figure 5 shows the (A) max. P_A and (B) corresponding U and (C) R_i of stack and (D) OCV varying with temperature. As shown in **Figure 4**, the temperature can effectively increase the OCV and reduce the R_i, thus increasing the Max. P_A of the stack. This is demonstrated by **Eqs 6**, **7**. The effect of temperature on the electromotance of the stack can be predicted using the Nernst equation. The electromotive force of the membrane increases with the increase of temperature. In practical experiments, due to the limited thermal stability of the ion exchange membrane, too high a temperature will have an irreversible impact on the polymer materials and ionic groups. Therefore, the effect of temperature on the Max. P_A of the stack is limited. As shown in **Figure 5B**, the corresponding U range at the Max. P_A is enlarged as the temperature increases. As shown in **Figure 5D**, from the OCV, 35°C is a more reasonable temperature.

3.2.3 Influence of Concentration

Figure 6 shows the (A) max. P_A and (B) corresponding U and (C) R_i of stack and (D) OCV varying with concentration. Increasing the salinity gradient energy (SGE) between solutions can increase the Gibbs energy between solutions. As shown in **Figure 6A**, under low SGE, the Max. P_A of all experimental groups is very small; the Max. P_A increases with the SGE increases. As shown in **Figure 6B**, with the increase of SGE, the corresponding U to the Max. P_A also shows an upward trend. As shown in **Figures 6C,D**, increasing the SGE between the feed solutions can reduce the R_i and increase the OCV. This is due to the fact that the R_i of the stack is high and more sensitive when the SGE is low. In addition, Mg^{2+} in feed solution makes the sensitivity of R_i and OCV decrease.

4 CONCLUSION

In this work, the effects of trace ions in concentrated brine and seawater on the performance of RED stack are experimentally studied by preparing NaCl solution with the same concentration and containing trace ions. The principal conclusions are as follows.

Multivalent ions in feed solutions will reduce the OCV and P_A, and increase the R_i of the RED stack, especially for multivalent cations. The influence of ions on the performance relates to salinity gradient. A greater SGE between concentrated solution and dilute solution means a greater OCV, Max. P_A, and a smaller R_i. Increasing the Φ of feed solutions can maintain the stability of SGP in the compartment and improve the output performance of the stack. However, excessive Φ will cause R_i to become unstable. Increasing feed temperature can improve the performance of the stack, but too high a temperature will damage the performance of the ion exchange membrane. Therefore, an appropriate feed temperature should be carefully considered according to the properties of the ion exchange membrane.

DATA AVAILABILITY STATEMENT

The original contributions presented in the study are included in the article/Supplementary Material, further inquiries can be directed to the corresponding author.

AUTHOR CONTRIBUTIONS

Author 1: ZW Software, Validation, Investigation, Data Curation, Writing—Original Draft Author 2: JL Conceptualization, Methodology, Software, Investigation, Data Curation,

Writing—Original Draft, Writing—Review and Editing, Funding acquisition Author 3: HW Software, Validation, Investigation, Data Curation, Writing—Original Draft Author 4: ML Validation, Investigation, Data Curation Author 5: LW Validation, Investigation, Data Curation, Author 6: XK Writing—Review and Editing, Supervision, Project administration, Funding acquisition.

FUNDING

This work is supported by Natural Science Foundation of Shandong Province of China (ZR2020QE208), Key Laboratory of Ocean Energy Utilization and Energy Conservation (Dalian University of Technology), and National Natural Science Foundation of China (No. 51776115).

REFERENCES

Achilli, A., and Desalination, A. C. J. (2010). Pressure retarded osmosis: from the vision of sidney loeb to the first prototype installation – review. *Desalination* 261, 205–211. doi:10.1016/j.desal.2010.06.017

Avci, A. H., Sarkar, P., Tufa, R. A., Messana, D., Argurio, P., Fontananova, E., et al. (2016). Effect of Mg^{2+} ions on energy generation by reverse electrodialysis. *J. Membr. Sci.* 520, 499–506. doi:10.1016/j.memsci.2016.08.007

Avci, A. H., Tufa, R. A., Fontananova, E., Di Profio, G., and Curcio, E. (2018). Reverse electrodialysis for energy production from natural river water and seawater. *Energy* 165, 512–521. doi:10.1016/j.energy.2018.09.111

Choi, J., Kim, W.-S., Kim, H. K., Yang, S. C., Han, J. H., Jeung, Y. C., et al. (2022). Fouling behavior of wavy-patterned pore-filling membranes in reverse electrodialysis under natural seawater and sewage effluents. *npj Clean. Water* 5, 6. doi:10.1038/s41545-022-00149-2

Chon, K., Jeong, N., Rho, H., Nam, J. Y., Jwa, E., and Cho, J. (2020). Fouling characteristics of dissolved organic matter in fresh water and seawater compartments of reverse electrodialysis under natural water conditions. *Desalination* 496, 114478. doi:10.1016/j.desal.2020.114478

Guo, Z.-Y., Ji, Z.-Y., Zhang, Y.-G., Yang, F. J., Liu, J., Zhao, Y. Y., et al. (2018). Effect of ions (K^+, Mg^{2+}, Ca^{2+} and SO_4^{2-}) and temperature on energy generation performance of reverse electrodialysis stack. *Electrochimica Acta* 290, 282–290. doi:10.1016/j.electacta.2018.09.015

Helfer, F., Lemckert, C., and Anissimov, Y. G. J. J. o. M. S. (2014). Osmotic power with pressure retarded osmosis: theory, performance and trends – a review. *J. Memb. Sci.* 453, 337–358. doi:10.1016/j.memsci.2013.10.053

Hong, J. G., Zhang, W., Luo, J., and Chen, Y. (2014). Corrigendum to "Modeling of power generation from the mixing of simulated saline and freshwater with a reverse electrodialysis system: the effect of monovalent and multivalentions". *Appl. Energy* 129, 398–399. doi:10.1016/j.apenergy.2014.05.051

Hu, J., Xu, S., Wu, X., Wang, S., Zhang, X., Yang, S., et al. (2020). Experimental investigation on the performance of series control multi-stage reverse electrodialysis. *Energy Convers. Manag.* 204, 112284. doi:10.1016/j.enconman.2019.112284

Hu, J., Xu, S., Wu, X., Wu, D., Jin, D., Wang, P., et al. (2019). Exergy analysis for the multi-effect distillation - reverse electrodialysis heat engine. *Desalination* 467, 158–169. doi:10.1016/j.desal.2019.06.007

Hulme, A. M., Davey, C. J., Parker, A., Williams, L., Tyrrel, S., Jiang, Y., et al. (2020). Managing power dissipation in closed-loop reverse electrodialysis to maximise energy recovery during thermal-to-electric conversion. *Desalination* 496, 114711. doi:10.1016/j.desal.2020.114711

Jang, J., Kang, Y., Han, J.-H., Jang, K., Kim, C. M., and Kim, I. S. (2020). Developments and future prospects of reverse electrodialysis for salinity gradient power generation: influence of ion exchange membranes and electrodes. *Desalination* 491, 114540. doi:10.1016/j.desal.2020.114540

Jianbo, L., Chen, Z., Kai, L., Li, Y., and Xiangqiang, K. (2021). Experimental study on salinity gradient energy recovery from desalination seawater based on RED. *Energy Convers. Manag.* 244, 114475. doi:10.1016/j.enconman.2021.114475

Jin, D., Xi, R., Xu, S., Wang, P., and Wu, X. (2021). Numerical simulation of salinity gradient power generation using reverse electrodialysis. *Desalination* 512, 115132. doi:10.1016/j.desal.2021.115132

Kang, S., Li, J., Wang, Z., Zhang, C., and Kong, X. (2022). Salinity gradient energy capture for power production by reverse electrodialysis experiment in thermal desalination plants. *J. Power Sources* 519, 230806. doi:10.1016/j.jpowsour.2021.230806

Kim, H., Yang, S., Choi, J., Kim, J. O., and Jeong, N. (2021). Optimization of the number of cell pairs to design efficient reverse electrodialysis stack. *Desalination* 497, 114676. doi:10.1016/j.desal.2020.114676

Mei, Y., and Tang, C. Y. (2017). Co-locating reverse electrodialysis with reverse osmosis desalination: synergies and implications. *J. Membr. Sci.* 539, 305–312. doi:10.1016/j.memsci.2017.06.014

Merino-Garcia, I., and Velizarov, S. (2021). New insights into the definition of membrane cleaning strategies to diminish the fouling impact in ion exchange membrane separation processes. *Sep. Purif. Technol.* 277, 119445. doi:10.1016/j.seppur.2021.119445

Moreno, J., Díez, V., Saakes, M., and Nijmeijer, K. (2018). Mitigation of the effects of multivalent ion transport in reverse electrodialysis. *J. Membr. Sci.* 550, 155–162. doi:10.1016/j.memsci.2017.12.069

Moya, A. A. (2017). A Nernst-Planck analysis on the contributions of the ionic transport in permeable ion-exchange membranes to the open circuit voltage and the membrane resistance in reverse electrodialysis stacks. *Electrochimica Acta* 238, 134–141. doi:10.1016/j.electacta.2017.04.022

Ngai, Y. Y., and Menachem, E. (2012). Thermodynamic and energy efficiency analysis of power generation from natural salinity gradients by pressure retarded osmosis. *Environ. Sci. Technol.* 46, 5230–5239. doi:10.1021/es300060m

Ortiz-Imedio, R., Gomez-Coma, L., Fallanza, M., Ortiz, A., Ibanez, R., and Ortiz, I. (2019). Comparative performance of salinity gradient power-reverse electrodialysis under different operating conditions. *Desalination* 457, 8–21. doi:10.1016/j.desal.2019.01.005

Pintossi, D., Chen, C.-L., Saakes, M., Nijmeijer, K., and Borneman, Z. (2020). Influence of sulfate on anion exchange membranes in reverse electrodialysis. *npj Clean. Water* 3, 29–10. doi:10.1038/s41545-020-0073-7

Pintossi, D., Simões, C., Saakes, M., Borneman, Z., and Nijmeijer, K. (2021). Predicting reverse electrodialysis performance in the presence of divalent ions for renewable energy generation. *Energy Convers. Manag.* 243, 114369. doi:10.1016/j.enconman.2021.114369

Post, J., Hamelers, W, H., Buisman, V, M, C., and J, N. (2008). Energy recovery from controlled mixing salt and fresh water with a reverse electrodialysis system. *Environ. Sci. Technol.* 42, 5785–5790. doi:10.1021/es8004317

Post, J. W., Hamelers, H. V. M., and Buisman, C. J. N. (2009). Influence of multivalent ions on power production from mixing salt and fresh water with a reverse electrodialysis system. *J. Membr. Sci.* 330, 65–72. doi:10.1016/j.memsci.2008.12.042

Rijnaarts, T., Huerta, E., van Baak, W., and Nijmeijer, K. (2017). Effect of divalent cations on RED performance and cation exchange membrane selection to enhance power densities. *Environ. Sci. Technol.* 51, 13028–13035. doi:10.1021/acs.est.7b03858

Roldan-Carvajal, M., Vallejo-Castaño, S., Álvarez-Silva, O., Bernal-Garcia, S., Arango-Aramburo, S., Sanchez-Saenz, C. I., et al. (2021). salinity gradient power by reverse electrodialysis: a multidisciplinary assessment in the colombian context. *Desalination* 503, 114933. doi:10.1016/j.desal.2021.114933

Simões, C., Pintossi, D., Saakes, M., Borneman, Z., Brilman, W., and Nijmeijer, K. (2020). Electrode segmentation in reverse electrodialysis: improved power and energy efficiency. *Desalination* 492, 114604–114612. doi:10.1016/j.desal.2020.114604

Tedesco, M., Cipollina, A., Tamburini, A., and Micale, G. (2017). Towards 1 kW power production in a reverse electrodialysis pilot plant with saline waters and concentrated brines. *J. Membr. Sci.* 522, 226–236. doi:10.1016/j.memsci.2016.09.015

Tufa, R. A., Pawlowski, S., Veerman, J., Bouzek, K., Fontananova, E., di Profio, G., et al. (2018). Progress and prospects in reverse electrodialysis for salinity gradient energy conversion and storage. *Appl. Energy* 225, 290–331. doi:10.1016/j.apenergy.2018.04.111

Vermaas, D. A., Kunteng, D., Saakes, M., and Nijmeijer, K. (2013). Fouling in reverse electrodialysis under natural conditions. *Water Res.* 47, 1289–1298. doi:10.1016/j.watres.2012.11.053

Vermaas, D. A., Saakes, M., and Nijmeijer, K. (2011). Doubled power density from salinity gradients at reduced intermembrane distance. *Environ. Sci. Technol.* 45, 7089–7095. doi:10.1021/es2012758

Vermaas, D. A., Saakes, M., and Nijmeijer, K. (2011). Power generation using profiled membranes in reverse electrodialysis. *J. Membr. Sci.* 385 386, 234–242. doi:10.1016/j.memsci.2011.09.043

Vermaas, D. A., Veerman, J., Saakes, M., and Nijmeijer, K. (2014). Influence of multivalent ions on renewable energy generation in reverse electrodialysis. *Energy Environ. Sci.* 7, 1434–1445. doi:10.1039/c3ee43501f

Zhu, X., He, W., and Logan, B. E. (2015). Influence of solution concentration and salt types on the performance of reverse electrodialysis cells. *J. Membr. Sci.* 494, 154–160. doi:10.1016/j.memsci.2015.07.053

Conflict of Interest: The authors declare that the research was conducted in the absence of any commercial or financial relationships that could be construed as a potential conflict of interest.